Pergamon

Geochimica et Cosmochimica Acta, Vol. 68, No. 8, pp. 1807–1813, 2004

0016-7037/04 $30.00 + .00

doi:10.1016/j.gca.2003.10.022

A vibrational spectroscopic study of the oxidation of pyrite by molecular oxygen

Michael J. Borda,[1,*,†] Daniel R. Strongin,[2] and Martin A. Schoonen[1]

[1]Department of Geosciences, The State University of New York at Stony Brook, Stony Brook, NY 11794-2100, USA
[2]Department of Chemistry, Temple University, Philadelphia, PA 19122, USA

(*Received March* 4, 2003; *accepted in revised form October* 21, 2003)

Abstract—In situ flow-through attenuated total reflectance (ATR) Fourier transform infrared (FTIR) spectroscopy has been used to investigate the formation, and step-wise oxidation, of sulfoxyanions at the pyrite surface during oxidation by molecular oxygen. The surface was studied under two different pH regimes (pH 2.5 and pH 5.6) and under two light conditions (dark and ultraviolet light). It was experimentally observed that multiple sulfoxyanions were present at the pyrite surface during oxidation by molecular oxygen, spectroscopically illustrating the concept of sulfur step-wise oxidation. The results from photochemical experiments were complex and suggest a dependence on both pH and surface speciation. *Copyright © 2004 Elsevier Ltd*

1. INTRODUCTION

The oxidation of pyrite (FeS_2) occurs over a range of pH conditions and primarily by two oxidants, ferric iron (Fe^{3+}) and molecular oxygen (O_2) (Eqns. 1 and 2, respectively).

$$FeS_2 + 14Fe^{3+} + 8H_2O \rightarrow 15Fe^{2+} + 16H^+ + 2SO_4^{2-} \quad (1)$$

$$FeS_2 + 3.5O_2 + H_2O \rightarrow Fe^{2+} + 2H^+ + 2SO_4^{2-} \quad (2)$$

At both low (<3.5) and high (>3.5) pH values, O_2 is an effective oxidant; however, in the low pH regime Fe^{3+} is the dominant oxidant (Eqn. 1) (Bonnissel-Gissinger et al., 1998). Recently, Borda et al. (2003b) studied the oxidation of pyrite by Fe^{3+} using attenuated total reflectance (ATR) Fourier transform infrared (FTIR) spectroscopy. This study focused on the step-wise oxidation of the disulfide (S_2^{2-}) group. Using a flow-through ATR reaction cell and a photochemical flow-through ATR reaction cell, the oxidation of pyrite under both dark conditions and under illumination with visible and ultraviolet light was investigated. This prior study showed the presence of multiple adsorbed sulfoxyanions at the pyrite surface during oxidation by Fe^{3+}. In that study, sulfate, in an outer-sphere complex, and thiosulfate, in a monodentate complex, were experimentally observed within a complex spectral result that suggested additional S-O species contributed to the surface speciation during oxidation.

The concept of the step-wise oxidation of S_2^{2-} is not new. Researchers have postulated the presence of intermediate sulfur species during the oxidation of pyrite and have directly measured aqueous concentrations of sulfoxyanions during these reactions (Steger and Desjardines, 1978; Goldhaber, 1983). However, until recently the direct spectroscopic observation of these intermediate species, in situ and in real time, has not been achieved (Borda et al., 2003b).

To develop a better understanding of the step-wise oxidation of the disulfide group under different pH regimes, i.e., pH values greater than and less than 3.5, this contribution reports the results of an ATR-FTIR spectroscopic analysis of pyrite oxidation by O_2. Both dark and illuminated conditions were investigated at pH 2.5 and 5.6. The focus of the ATR-FTIR analysis is on the wavenumber region from 950 to 1250 cm^{-1}, the region associated with the vibrational modes of S-O bands in sulfoxyanions.

The strength of the ATR-FTIR technique is that it is intrinsically surface sensitive. Using ATR, spectra are collected only from absorptions of an evanescent wave with a maximum penetration depth of several micrometers away from the internal reflection element into the solution phase (Harrick, 1967). This short optical path length allows one to limit the absorption due to an aqueous phase associated with the sample, but also to have a high sensitivity to species at the mineral–water interface (McQuillan, 2001). Using sample particles that are on the same length scale as the depth of penetration of the evanescent wave and directly depositing them onto the ATR crystal achieve this high surface sensitivity.

In formulating a mechanism for the oxidation of pyrite by O_2, important prior observations must be considered (Goldhaber, 1983; McKibben and Barnes, 1986; Luther, 1987; Moses et al., 1987; Nicholson et al., 1988; Nesbitt and Muir, 1994; Williamson and Rimstidt, 1994; Guevremont et al., 1998; Kamei and Ohmoto, 2000; Schoonen et al., 2000). Rosso et al. (1999) investigated the interaction between pyrite and O_2 using scanning tunneling microscopy and scanning tunneling spectroscopy (STM-STS) complemented by ab initio calculations, and Becker et al. (2001) recently reviewed the work in the context of the proximity effect. Both Rosso et al. (1999) and Becker et al. (2001) conclude that the initial step in the reaction of pyrite with O_2 is the dissociative adsorption of O_2 at Fe sites on the surface producing Fe-O groups. The Fe-O groups are then predicted to distort the local electron density at surrounding Fe and S sites. Recent research also has shown that the reaction of water with pyrite leads to the formation of hydrogen peroxide that may be involved in reaction with S groups, producing S-O step-wise oxidation products consistent with previous pathways proposed for pyrite oxidation by Fe^{3+} (Wiersma and Rimstidt, 1984; Luther, 1987; Moses et al., 1987; Williamson and Rimstidt, 1994; Guevremont et al., 1998).

* Author to whom correspondence should be addressed (mborda@udel.edu).
† *Present address:* Department of Plant and Soil Sciences, The University of Delaware, Newark, DE 19716-2701

Borda et al. (2003b) suggested that the final step-wise reaction generates SO_4^{2-} that remains initially adsorbed in an outer-sphere complex. This allows for the transfer of 7 electrons, through reaction steps, converting S^{1-} (disulfide) to S^{6+} (sulfate) while electrons are being withdrawn by oxidants at Fe sites (Biegler and Swift, 1979). These reactions are consistent with isotopic work done previously that demonstrates a majority of the sulfate generated during pyrite oxidation derives its oxygen signature from H_2O rather than from O_2 (Taylor et al., 1984; Reedy et al., 1991). This does not imply that H_2O is the electron acceptor in the system, but rather that H_2O acts as a vehicle for electron transfer ultimately to O_2 or Fe^{3+}.

We hypothesize that although the initial oxidation step differs when O_2 or Fe^{3+} react with pyrite, as nucleophilic attack begins, the step-wise oxidation of the disulfide group should follow the same progression regardless of the oxidant. Using ATR-FTIR spectroscopy this hypothesis has been studied.

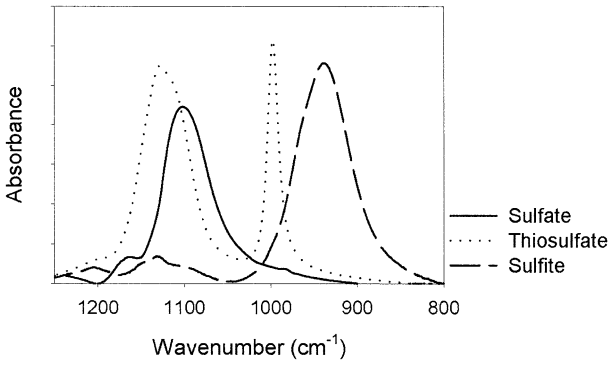

Fig. 1. Reference spectra for solution phase, 0.5 mol/L solutions, of sulfate (solid), thiosulfate (dotted), and sulfite (dashed) collected on a Ge ATR crystal.

2. EXPERIMENTAL METHODS

The general methods used in this report for both the flow-through ATR-FTIR and flow-through photochemical ATR-FTIR techniques have recently been described in Borda et al. (2003b) and Borda et al. (2003a), respectively. Briefly, two different cell designs can be utilized to perform in situ vibrational spectroscopic measurements on hydrothermally synthesized pyrite (250 g/L) that was dried on a germanium (Ge) ATR crystal. The pyrite used has a grain size of approximately 900 nm. One cell is capable of flow-through type reactions, whereas the other cell is capable of flow-through type reactions along with the introduction of ultraviolet (200–400 nm) light into the system via a fiberoptic equipped deuterium light source. Spectra are collected in real time, and the extraction of peak height vs. time data allows for kinetic measurements to be obtained. Due to a large number of spectra collected for each experimental run (>100), only a representative spectral set is shown for clarity.

The experiments were run by first coating the Ge ATR crystal with 10 L of the 250 g/L pyrite slurry in a glove box under N_2. All solutions, which were in contact with the pyrite before the actual introduction of O_2, were deoxygenated by N_2 purging for a minimum of 2 h. The oxic solution was purged with pure O_2 for a minimum of 2 h. Because pyrite oxidation by O_2 occurs over a range of pH values, each photochemical variable (dark and ultraviolet light) was tested in two different pH regimes, pH 2.5 and pH 5.6.

To overcome the relatively slow oxidation rates with O_2, the advected solution was heated so that measurable oxidation products formed within a reasonable reaction time (20–30 h). The reaction time dependence was based on the observation that colloidal pyrite films become unstable and may become dislodged from the ATR lens after exposure for greater than approximately 30 h. The deterioration of the film was evidenced by changes in the collected spectra. Once these spectral changes were observed, the experiment was terminated. For all of the reported experiments a solution temperature of 35 °C was used.

The unique assignment of multiple sulfoxyanion peaks is difficult, as illustrated in Borda et al. (2003b). Drawing on previous ATR-FTIR studies of sulfoxyanions (Gabelica, 1979; Persson and Lövgren, 1996; Hug, 1997; Peak et al., 1999), it is clear that a number of different species are necessary to fit the complex spectra collected during this study. Although complicated spectral fitting may extract some information from these spectra, the authors chose to limit the interpretation to peaks that were visually present and to make some speculation about species that are consistent with those visible peaks. Due to a high level of peak overlap and the potential of a large number of species being present at the surface, this approach appeared to be the most practical.

One important issue about assigning peaks using ATR-FTIR data is the choice of standard spectra for a specific adsorbed species. In this study, sulfoxyanion spectra were referenced from several prior studies, however, none of these studies adsorbed the specific sulfoxyanion to a pyrite surface. Because the vibrational energy is directly related, in a classical sense, to the force constant of the bond of interest, changes in vibrational modes can be interpreted as changes in the adsorption behavior of species as the force constants of bonds will change upon adsorption (Urban, 1996). With this in mind, adsorption to different surfaces will affect force constants differently and will cause subtle shifts in the absolute peak position of infrared bands collected. Therefore, when making comparisons to previous studies, it is instructive to keep in mind that the absolute peak positions may be somewhat different for species collected on different substrates. The number of peaks is derived from group theory based on the symmetry of the molecule of interest and is also instructive in the assignment of vibration spectra to adsorbed complexes (Nakamoto, 1986). High-quality spectra of sulfoxyanions are difficult to obtain on the pyrite surface, in a reference sense, due to the constantly changing surface as additional sulfur species were continuously being generated. Therefore, reference spectra from solution phase species coupled with group theory arguments and also spectra of sulfoxyanions adsorbed to model surfaces were used to interpret the results herein.

The assignment of peaks as surface species, without contribution from solution species, is facilitated by the concentration dependence of the ATR method. ATR-FTIR is a surface-sensitive technique due to the solution concentration required to allow aqueous species to be detected. It has been shown that a minimum concentration of approximately 1 mM is necessary for solution species to be detected using ATR-FTIR (Duckworth and Martin, 2001). With a flow-through system it is unlikely to reach solution concentrations greater than 1 mM, therefore species detected in our experiments are exclusively surface-bound S-O species.

To illustrate the peak positions for three of the most significant peaks in the spectra collected in this study, Figure 1 shows the infrared spectra for solution-phase free aqueous (0.5 mol/L solution) sulfate (SO_4^{2-}), sulfite (SO_3^{-}), and thiosulfate ($S_2O_3^{2-}$). Spectra were collected at the appropriate pH so that each of these species was in the fully deprotonated form.

2.1. Dark Flow-Through Experiments

In the dark flow-through experiments, a background spectrum was collected with a continuous flow of deoxygenated DI water of the appropriate pH (2.5 or 5.6). Once a stable background was collected, oxygenated solution flowed continuously over the ATR lens containing deposited pyrite. Spectra were collected every 30 min for the duration of the experiment.

2.2. Photochemical Flow-Through Experiments

Photochemical experiments followed the method previously reported in Borda et al. (2003a). A background spectrum was collected with a continuous flow of deoxygenated DI water adjusted to the pH conditions chosen for the experiment. Once a stable background was collected, oxygenated solution was passed through the cell and the ultra-

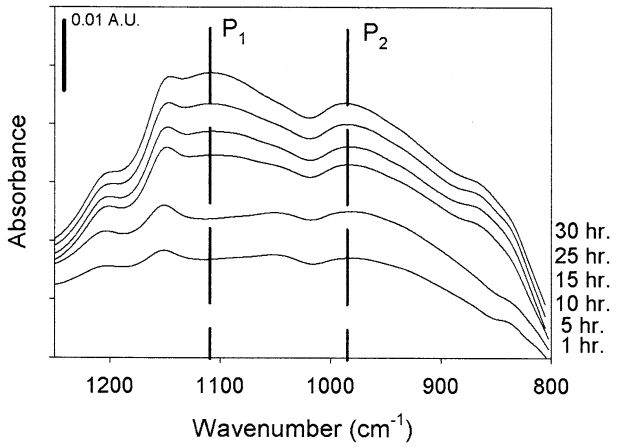

Fig. 2. Spectra collected over 30 h of exposure of FeS_2 to pure O_2 at pH 2.5 in the dark using the flow-through method. P_1 (1110 cm^{-1}) and P_2 (990 cm^{-1}) represent the most prominent peaks in the spectra. Spectra are offset in absorbance for clarity.

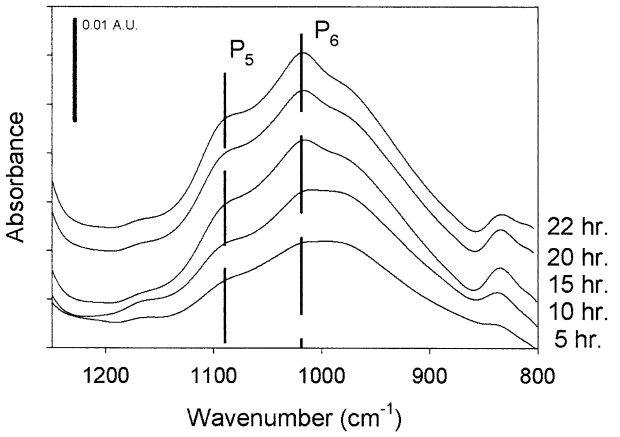

Fig. 4. Spectra collected over 22 h of exposure of FeS_2 to pure O_2 at pH 2.5 using the flow-through method and illumination with ultraviolet light. P_6 (1010 cm^{-1}) represents the most prominent peak in the spectra and P_5 (1090 cm^{-1}) is shown for reference within the broad shoulder. Spectra are offset in absorbance for clarity.

violet light source was switched on. The light remained on for the duration of the experiment, and a spectrum was collected every 30 min.

3. RESULTS

3.1. Dark Flow-Through Experiments

The results of the dark oxidation experiments at pH 2.5 and pH 5.6 are shown in Figures 2 and 3, respectively. There are clearly discernable differences between the two sets of spectra. The pH 2.5 spectrum shows two peaks; P_1 is broad and shows two peak maxima, one at 1110 cm^{-1} and a second at 1150 cm^{-1}, and P_2 has a peak center located at 990 cm^{-1}. The spectra show a peak intensity ratio of P_1:P_2 near 1:1 and show significant broadening at both the high and low wavenumber ends of the spectra. There is a distinguishable peak at 1200 cm^{-1} and shoulder at 880 cm^{-1}.

The pH 5.6 spectra show a different peak structure. The spectra show two peaks. P_3 is distinct and shows peak maxima at 1100 cm^{-1}. P_2 is a shoulder with a small peak center located at 995 cm^{-1}. The P_3:P_4 peak intensity ratio is nearly 2:1 and there is little broadening at the high wavenumber end of the spectra. There is a shoulder at the low wavenumber end of the spectra, although there are no distinct peaks. The experiments for pH 2.5 and pH 5.6 were run for 30 h and 22 h, respectively.

3.2. Photochemical Flow-Through Experiments

The results of the ultraviolet light oxidation experiments at pH 2.5 and pH 5.6 are shown in Figures 4 and 5, respectively. The pH 2.5 spectra show the most dramatic differences from the dark spectra. P_6 has a peak center at approximately 1010 cm^{-1} and a broad shoulder on the low wavenumber side. P_5 is labeled for convenience and represents the shoulder located near 1090 cm^{-1}. The most dramatic change from the dark spectra is the change in peak intensity ratio from 1:1 (P_1:P_2) to approximately 1:2 (P_5:P_6).

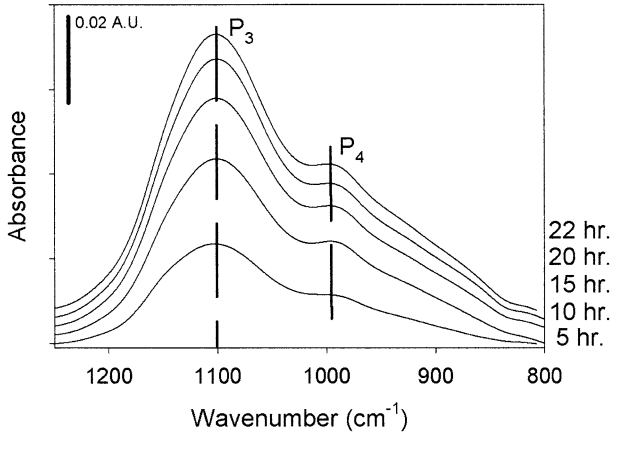

Fig. 3. Spectra collected over 22 h of exposure of FeS_2 to pure O_2 at pH 5.6 in the dark using the flow-through method. P_3 (1100 cm^{-1}) and P_4 (995 cm^{-1}) represent the most prominent peaks in the spectra. Spectra are offset in absorbance for clarity.

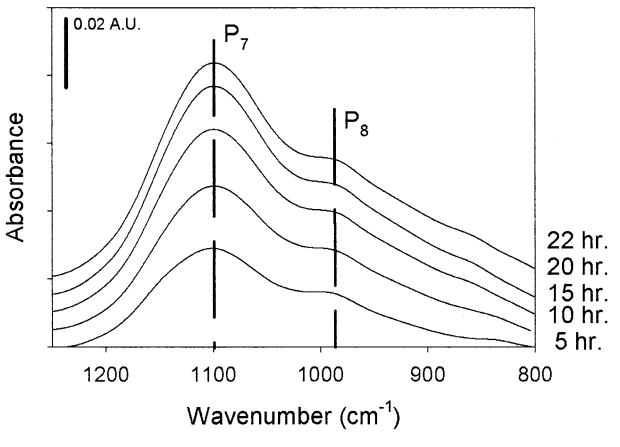

Fig. 5. Spectra collected over 22 h of exposure of FeS_2 to pure O_2 at pH 5.6 using the flow-through method and illumination with ultraviolet light. P_7 (1105 cm^{-1}) and P_8 (990 cm^{-1}) represent the most prominent peaks in the spectra. Spectra are offset in absorbance for clarity.

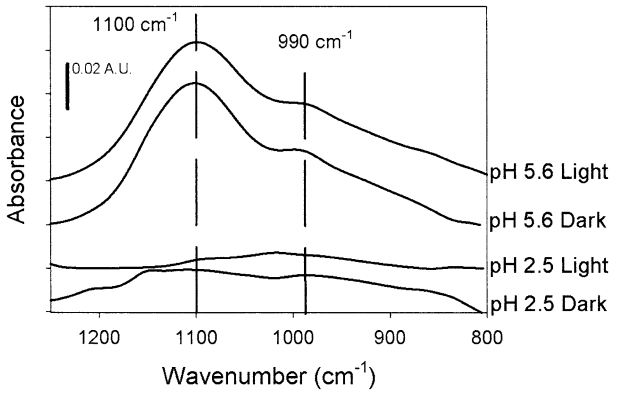

Fig. 6. Plot of the final spectrum collected under each experimental condition for the comparison of peak changes. Spectra were collected over different time spans: pH 2.5 dark (30 h), pH 5.6 dark (22 h), pH 5.6 ultraviolet light (22 h), pH 2.5 ultraviolet light (22 h).

The pH 5.6 spectra have a well-developed peak at 1100 cm^{-1} (P_7) and a broad shoulder with peak intensity at 990 cm^{-1} (P_8). The peak intensity ratio of P_7:P_8 is approximately 2:1. Both experiments at pH 2.5 and pH 5.6 were run for 22 h. Figure 6 shows the final spectrum collected for each experimental condition to better illustrate the changes in peak shape.

4. DISCUSSION

Previously, Borda et al. (2003b) reported the in situ characterization of step-wise sulfur oxidation products at the pyrite surface during oxidation by Fe^{3+}. The spectra collected in the present study show a similar degree of complexity as those previously reported. Figure 6 displays the longest oxidation time spectrum for each experimental condition used in this study and emphasizes the significant asymmetry of each peak shape, suggesting that more than a single surface species exists on the pyrite surface under all of the different experimental conditions.

It is useful from the onset to briefly discuss the characteristic frequency positions for vibrations associated with potential sulfoxyanions (Table 1). Two important species that may be present during pyrite oxidation are sulfate and thiosulfate. The antisymmetric (v_3) vibrational mode for sulfate with a distorted T_d symmetry (outer sphere) is centered at 1110 cm^{-1} (Fig. 1). Sulfate in the lowered symmetry forms, associated with monodentate (C_{3v}) and bidentate (C_{2v}) complexes, show an increasing number of peaks and shifting peak positions. These characteristic vibrational frequency positions are illustrated in a prior work by Hug (1997).

The symmetric (v_1) vibrational mode for thiosulfate in a monodentate complex is centered at 1000 cm^{-1}. Thiosulfate also has spectral weight at 1130 cm^{-1} (v_3) with a peak ratio ($v_{3:n1}$) of approximately 1:1. Two additional species that may be present at an oxidized pyrite surface are sulfite (SO_3^{2-}) and bisulfate (HSO_4^-). The highest intensity sulfite peak is centered at 930 cm^{-1} (v_3). Bisulfate in an outer-sphere surface complex shows peak intensities at 890 cm^{-1} and 1210 cm^{-1} (Hug, 1997).

To use the spectral data collected to develop a rate for oxidation, relative peak height growth was determined. Making semiquantitative comparisons of peaks associated with different species requires that the relative molar absorptivity of the individual species be known. From solution concentration vs. peak height data, the molar absorptivities for thiosulfate and sulfate were experimentally determined and have been shown to reflect equivalent surface concentrations with equivalent peak heights (Borda et al., 2003b).

4.1. Dark Flow-Through Experiments

Pyrite oxidation in the low and high pH regimes produce markedly different spectra. At low pH (<3.5), significant broadening of the spectra is experimentally observed. The presence of peaks at 1210 cm^{-1} and 860 cm^{-1} suggests that a significant amount of bisulfate is present at the surface. This interpretation is entirely consistent with the pH conditions within the experiment. Though the inflow solution pH was 2.5, the pH of solution directly at the mineral–water interface may be somewhat lower due to the production of H^+ at the surface during oxidation. The second acid dissociation constant (pK_2) for H_2SO_4 is 1.9, making it plausible for bisulfate to be in significant concentration at the surface. The presence of bisulfate will also diminish the peak intensity of sulfate due to the presence of two S(VI) species with different spectral signa-

Table 1. The positions of peak maxima of selected sulfoxyanions in coordination complexes relevant to this study.[a]

Sulfoxyanion	Sulfur oxidation state	Coordination	v_1 (cm^{-1})	v_3 (cm^{-1})
Sulfate[c]	VI	Outer-sphere	NA or 975	1100–1140
Sulfate[b]	VI	Monodentate	975	1050, 1160
Sulfate[b]	VI	Bidentate	975–1000	1075, 1175, 1210
Bisulfate[b]	VI	Outer-sphere	890	1040, 1210
Sulfite[c]	IV	Monodentate	930	1130
Thiosulfate[d]	II	Monodentate	1000	1130
Thiosulfate[d]	II	Bridging	1030	1200

[a] Data taken from the literature (Gabelica, 1979; Hug, 1997) and obtained in our laboratory. Data from Hug (1997) were collected as follows: monodentate SO_4^{2-} (C_{3v}) was collected on goethite, bidentate SO_4^{2-} (C_{2v}) was collected on hematite, and HSO_4^- (C_{3v}) was collected as a free aqueous species. Data from Gabelica (1979) were collected on cadmium thiosulfate complexes. Free aqueous SO_4^{2-} (T_d) was determined in our laboratory for this study using a 0.5 M Na_2SO_4 solution and is comparable to the literature reported values.
[b] Hug, 1997.
[c] This study.
[d] Gabelica, 1979.

tures. This may explain the low peak ratio of P_1:P_2 (1:1) in Figure 2.

An implication of having a significant amount of bisulfate sequestered at the pyrite surface can be illustrated through an acid mine drainage scenario. Mine tailing piles are often exposed to periodic fluxes of rainwater. If a significant amount of bisulfate is present and mobilized instantaneously during a precipitation event, high concentrations of acidity may be released into the environment with potentially detrimental effects.

At higher pH, bisulfate is absent and the spectra show a P_3:P_4 ratio of 2:1. This suggests that P_3 (1105 cm^{-1}) is associated with the presence of sulfate. With a peak position close to 1110 cm^{-1}, sulfate would be assigned to the distorted T_d symmetry, characteristic of an outer-sphere sulfate surface complex. No additional peaks are associated with that type of complex, so a second species is necessary to characterize P_4. Thiosulfate in a monodentate surface complex shows spectral intensity at 1000 cm^{-1}, consistent with P_4. Associated with that symmetry is a peak centered at 1130 cm^{-1} (Gabelica, 1979). Such a contribution may be contained within the relatively broad P_3 feature.

These data suggest that in dark flow-through experiments, sulfate and thiosulfate are, at least in part, present as surface species. Under low pH conditions, bisulfate is an important surface species, presumably due to the higher proton concentration in solution in proximity to the mineral surface.

4.2. Photochemical Flow-Through Experiments

The effect of illumination on pyrite oxidation is complex and may be dependant on both solution and surface chemistry. The observed effects may be due to the more facile release of sulfate into solution with the presence of light or to a change in the pyrite surface properties. The release of sulfate may be explained by considering the change in activation energy on the basis of sulfate release data reported by Schoonen et al. (2000). This prior study reported no comparable increase when activation energies were calculated on the basis of Fe_{tot} release rates. Drawing on this different illumination dependence of activation energies derived from total iron and sulfate release rates, Schoonen et al. (2000) argued that the release of iron and sulfate are decoupled. This suggests that the release of iron and sulfate involve, at a minimum, two different reaction pathways, each with a different rate-limiting step. This result explains the activation energy difference on the basis of those two reaction progress variables (see Schoonen et al., 2000, their Fig. 11).

The results obtained in this study support the concept that the reaction pathway for sulfate is affected by illumination. Borda et al. (2003b) have experimentally observed this effect on the sulfur chemistry at the pyrite surface as a significant loss in spectral intensity associated with sulfate under illumination. The effect was observed with both ultraviolet and visible light, but in this prior study, only low pH conditions were evaluated because of iron solubility constraints.

In the present study, both low pH (2.5) and high pH (5.6) conditions were studied and a dependence on pH has been observed. In the pH 2.5 experiment with ultraviolet light, the peak intensity ratio P_5:P_6 is approximately 1:2 in contrast to the dark experiment with a P_1:P_2 ratio of 1:1. This suggests that the intensity of P_5 is diminished in the pH 2.5 experiment with respect to P_6 in the pH 5.6 experiment. This is consistent with the preferential loss of sulfate from the surface.

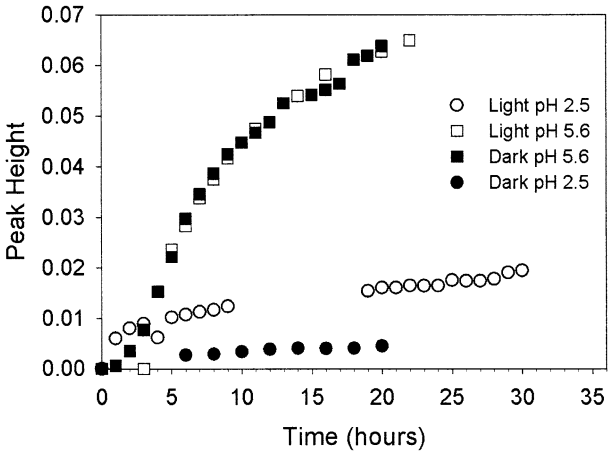

Fig. 7. Plot of the relative peak height of the 1110 cm^{-1} peak (sulfate) vs. time showing the relative rate of peak growth for each experimental condition. Open symbols represent experiments with ultraviolet light and closed symbols represent dark experiments.

Although sulfur species were the focus of this report, the fate of iron may play an important role in the surface chemistry under the higher pH (>3.5) conditions in specific experiments. At low pH (<3.5), Fe^{3+} is soluble; however, at higher pH, the pyrite surface becomes decorated with discrete Fe(III)-oxide patches (Eggleston et al., 1996). The formation of an Fe(III)-oxide patch may either inhibit photochemical reactions by distorting the electronic structure at the surface, or may potentially act as a site where sulfate can bind strongly to the surface. This interpretation is consistent with prior studies that show the adsorption of sulfate onto ferric oxides occurs readily (Zhang and Sparks, 1990).

At pH 5.6, with ultraviolet light, no change in the peak intensity ratio is observed with respect to the dark spectra. This suggests that either light is not having an effect at higher pH, or the surface has changed in a way that facilitates the adsorption of sulfate. We speculate that an increase in reactivity, due to illumination, would increase the formation and transgression of ferric oxide patches at the pyrite surface at higher pH. This would in turn create more available sites for sulfate adsorption and cause an increase in the 1100 cm^{-1}:1000 cm^{-1} peak intensity ratio.

Figure 7 is a plot of peak height vs. time based on the relative peak height of the 1100 cm^{-1} peak. This plot illustrates differences in the rate of sulfur species growth on the pyrite surface. There is a dramatic difference in the rate between the pH 5.6 and pH 2.5 experiments that may result from two competing mechanisms. First, because of the presence of bisulfate, the rate based on the growth of the 1100 cm^{-1} peak may not accurately represent the total amount of S(VI) being generated. This mechanism does not completely explain the spectra however, because the hypothetical addition of the excess spectral weight contributed by bisulfate to the sulfate peak would not produce a peak large enough to match the pH 5.6 experiment. The second mechanism relies on the strong pyrite oxidation rate dependence on pH (Schoonen et al., 2000). Therefore, it is reasonable to expect that the slower rate for the low

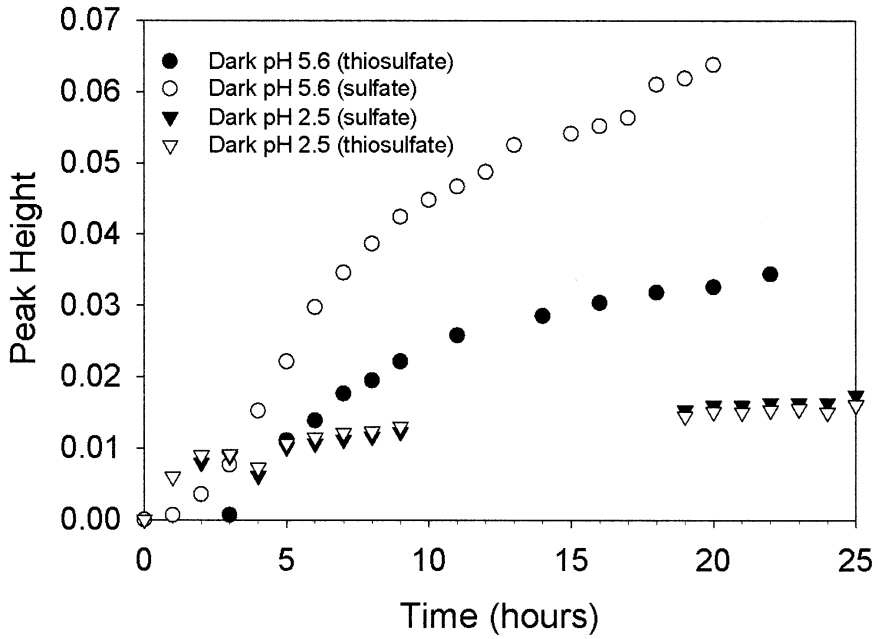

Fig. 8. A plot showing the relative rates calculated from both the sulfate peak ((1100 cm^{-1}) and thiosulfate peak ((1000 cm^{-1}) of the pH 5.6 dark oxidation experiment and the pH 2.5 dark oxidation experiment.

pH experiment expressed in Figure 7 based on peak height vs. time data is reasonable. This effect of pH and multiple S(VI) surface species may also explain the discrepancy in the measure of rates between the dark and ultraviolet experiments. The rates shown for both the dark and ultraviolet light experiments at pH 5.6 show a remarkable correlation. Although the relative rates of sulfate production estimated from the ultraviolet and dark experiments at pH 5.6 are in good agreement, the sulfate peak may be measuring more than simply the relative production rate of sulfate through the oxidation reaction. As stated earlier, ferric oxides patches at pH levels above 3.5 may decorate the pyrite surface. Due to sorption of sulfate to these ferric oxide patches, the relative intensity of the 1100 cm^{-1} peak may more accurately measure the capacity for the oxide patches to adsorb sulfate than the rate of production of sulfate. This discrepancy may be avoided by looking at the relative rate of the growth of the 1000 cm^{-1} peak (thiosulfate).

By examining the relative rates that may be obtained by using the growth of the 1000 cm^{-1} peak, it can be seen that a significant increase in the amount of sulfate with respect to thiosulfate for higher pH experiments is found (Fig. 8). Experiments at low pH do not show this discrepancy between thiosulfate and sulfate and suggest that at the higher pH condition more sulfate is being adsorbed at the surface. The consistent presence of thiosulfate also verifies that under every condition investigated thiosulfate is included in the reaction sequence. The shape of the thiosulfate vs. time curve also suggests that the concentration of thiosulfate reaches a steady state through time.

Figure 9 illustrates the concept that the oxidation of the disulfide group is independent of oxidant. The overall peak shape between experiments run with Fe^{3+} and O_2 as oxidants is consistent, although there are subtle differences in the spectra that may be attributed to different pH conditions. Therefore, the sulfoxyanion species at the surface are expected to be similar.

5. CONCLUSION

The use of in situ flow-through ATR-FTIR spectroscopy was used to investigate the surface sulfoxyanions formed during the oxidation of pyrite by O_2. Though it was not possible to completely assign every sulfoxyanion that may be contributing to the spectra collected, the presence of at least two species is

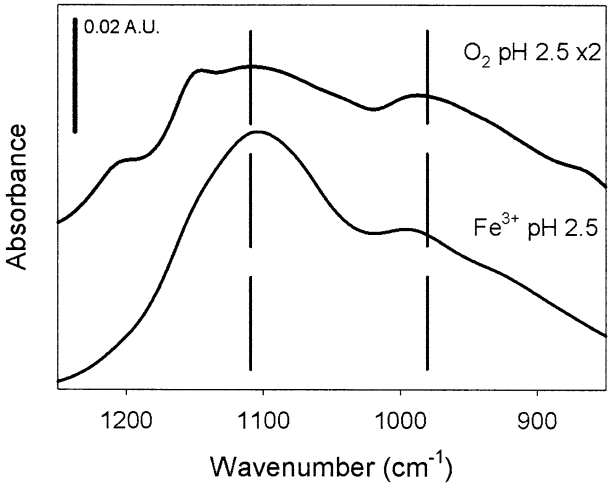

Fig. 9. A comparison plot of the final spectra collected for a dark oxidation experiment with Fe^{3+} (pH 2.5) and O_2 (pH 2.5) as oxidant, respectively. The oxygen spectrum was multiplied by 2x to be of comparative absorbance. The similarity in these two spectra suggests that the sulfur oxidation products are comparable with either oxidant.

in agreement with the step-wise oxidation pathways previously hypothesized. The presence of a sulfoxyanion consistent with thiosulfate as a precursor in all of the experiments spectroscopically verifies that the reaction sequence involves sulfur in intermediate oxidation states. In comparison to the results from a previous study of pyrite oxidation by Fe^{3+}, it is concluded that the step-wise oxidation of the disulfide group is independent of oxidant. The reported results also confirm that the mechanism for pyrite oxidation by O_2 is affected by light and by pH. These effects have not been fully explained; however, the characterization of the surface sulfoxyanions during this process is an important step forward. The ability to analyze the oxidizing surface in situ, and the capability to derive relative reaction kinetics, represents a substantial advance in pyrite oxidation studies.

Acknowledgments—M.A.S. and D.R.S greatly appreciate support from the Department of Energy, Basic Energy Sciences from grants DEFG029ER14633 and DEFG0296ER14644, respectively.

Associate editor: U. Becker

REFERENCES

Becker U., Rosso K. M., and Hochella M. F. (2001) The proximity effect on semiconducting mineral surfaces: A new aspect of mineral surface reactivity and surface complexation theory? *Geochim. Cosmochim. Acta* **65 (***16***),** 2641–2649.

Biegler T. and Swift D. A. (1979) Anodic behaviour of pyrite in acid solutions. *Electrochim. Acta* **24,** 415–420.

Bonnissel-Gissinger P., Alnot M., Ehrhardt J.-J., and Behra P. (1998) Surface oxidation of pyrite as a function of pH. *Environ. Sci. Technol.* **32,** 2839–2845.

Borda M. J., Strongin D. R., and Schoonen M. A. (2003a) A novel vertical attentuated total reflectance photochemical flow-through reaction cell for Fourier transform infrared spectroscopy. *Spectrochim. Acta, Part A: Molec. Spectrosc.* **59 (5),** 1103–1106.

Borda M. J., Strongin D. R. and Schoonen M. A. (2003b). A vibrational spectroscopic study of the oxidation of pyrite by ferric iron. *Am. Mineralogist.* **88,** 1318–1323.

Duckworth O. W. and Martin S. T. (2001) Surface complexation and dissolution of hematite by C-1-C-6 dicarboxylic acids at pH=5.0. *Geochim. Cosmochim. Acta* **65 (***23***),** 4289–4301.

Eggleston C. M., Ehrhardt J., and Stumm W. A. M. (1996) Surface structural controls on pyrite oxidation kinetics: An XPS-UPS, STM and modeling study. *Am. Mineralogist* **81,** 1036–1056.

Gabelica Z. (1979). Infrared and Raman investigation of the structural behavior of the $S_2O_3^{2-}$ ion in cadium thiosulfate dihydrate, $CdS_2O_3.2H_2O$. *Chem. Lett.* 1419–1422.

Goldhaber M. B. (1983) Experimental study of metastable sulfur oxyanion formation during pyrite oxydation at pH 6–9 and 30°C. *Am. J. Sci.* **283,** 193–217.

Guevremont J., Bebié J., Elsetinow A. R., Strongin D. R., and Schoonen M. A. A. (1998) Reactivity of the (100) plane of pyrite in oxidizing gaseous and aqueous environments: Effects of surface imperfections. *Environ. Sci. Technol.* **32,** 3743–3748.

Harrick N. J. (1967) *Internal Reflectance Spectroscopy*. John Wiley and Sons.

Hug S. J. (1997) In situ Fourier transform infrared measurements of sulfate adsorption on hematite in aqueous solutions. *J. Colloid Interface Sci.* **188 (***2***),** 415–422.

Kamei G. and Ohmoto H. (2000) The kinetics of reactions between pyrite and O_2-bearing water revealed in insitu monitoring of DO, Eh, and pH in a closed system. *Geochim. Cosmochim. Acta* **64 (***15***),** 2585–2601.

Luther G. W. (1987) Pyrite oxidation and reduction: Molecular orbital theory considerations. *Geochim. Cosmochim. Acta* **51,** 3193–3201.

McKibben M. and Barnes H. (1986) Oxidation of pyrite in low temperature acidic solutions: Rate laws and surface textures. *Geochim. Cosmochim. Acta* **50,** 1509–1520.

McQuillan A. J. (2001) Probing solid-solution interfacial chemistry with ATR-IR spectroscopy of particle films. *Advanced Materials* **13 (***12–13***),** 1034–1038.

Moses C. O., Nordstrom D. K., Herman J. S., and Mills A. L. (1987) Aqueous pyrite oxidation by dissolved oxygen and by ferric iron. *Geochim. Cosmochim. Acta* **51,** 1561–1572.

Nakamoto K. (1986) *Infrared and Raman Spectra of Inorganic and Coordination Compounds*. Wiley.

Nesbitt H. W. and Muir I. J. (1994) X-ray photoelectron spectroscopic study of a pristine pyrite surface reacted with water vapour and air. *Geochim. Cosmochim. Acta* **58,** 4667–4679.

Nicholson R. V., Gillham R. W., and Reardon E. J. (1988) Pyrite oxidation in carbonate-buffered solution: 1. Experimental kinetics. *Geochim. Cosmochim. Acta* **52,** 1077–1085.

Peak D., Ford R., and Sparks D. (1999) An in-situ ATR-FTIR investigation of sulfate bonding mechanisms on goethite. *J. Colloid Interface Sci.* **218,** 289–299.

Persson P. and Lövgren L. (1996) Potentiomentric and spectroscopic studies of sulfate complexation at the goethite-water interface. *Geochim. Cosmochim. Acta* **60 (***15***),** 2789–2799.

Reedy B. J., Beattie J. K., and Lowson R. T. (1991) A vibrational spectroscopic ^{18}O tracer study of pyrite oxidation. *Geochim. Cosmochim. Acta* **55,** 1609–1614.

Rosso K. M., Becker U., and Hochella M. F. J. (1999) The interaction of pyrite {100} surfaces with O_2 and H_2O: Fundamental oxidation mechanisms. *Am. Mineralogist* **84,** 1549–1561.

Schoonen M. A. A., Elsetinow A., Borda M. and Strongin D. R. (2000). Effect of temperature and illumination on pyrite oxidation between pH 2 and 6. *Geochem. Trans.* **4**.

Steger H. F. and Desjardines L. E. (1978) Oxidation of sulfide minerals. 4 Pyrite, chalcopyrite and pyrrhotite. *Chem. Geol.* **23,** 225–237.

Taylor B. E., Wheeler M. C., and Nordstrom D. K. (1984) Stable isotope geochemistry of acid mine drainage: Experimental oxidation of pyrite. *Geochim. Cosmochim. Acta* **48,** 2669–2678.

Urban M. W. (1996) *Attenuated Total Reflectance Spectroscopy of Polymers: Theory and Practice*. American Chemical Society.

Wiersma C. L. and Rimstidt J. D. (1984) Rates of reaction of pyrite and marcasite with ferric iron at pH 2. *Geochim. Cosmochim. Acta* **48,** 85–92.

Williamson M. A. and Rimstidt J. D. (1994) The kinetics and electrochemical rate-determining step of aqueous pyrite oxidation. *Geochim. Cosmochim. Acta* **58 (***24***),** 5443–5454.

Zhang P. C. and Sparks D. L. (1990) Kinetics and mechanisms of sulfate adsorption desorption on goethite using pressure-jump relaxation. *Soil Sci. Soc. Am. J.* **54 (***5***),** 1266–1273.